A Constrained Intersubmodule State-of-Charge Balancing Method for Battery Energy Storage Systems Based on the Cascaded H-Bridge Converter

Gaowen Liang, *Student Member, IEEE*, Ezequiel Rodriguez, *Student Member, IEEE*, Glen G. Farivar, *Senior Member, IEEE*, Salvador Ceballos, Christopher D. Townsend, *Member, IEEE*, Naga Brahmendra Yadav Gorla, *Member, IEEE*, and Josep Pou, *Fellow, IEEE*

***Abstract*—In the operation of battery energy storage systems (BESSs) based on the cascaded H-bridge (CHB) converters, it is desirable to balance the state of charge (SoC) among the submodules (SMs) within each phase arm. However, there are constraints on the active power distribution among the SMs that intend to balance the SoC. For instance, each SM in a practical system is designed with a specific power rating and can be damaged if it is exceeded. Therefore, a novel rule-based method is proposed in this article to achieve a fast SoC balancing, while respecting the power constraints of the SMs. The proposed method is general and readily applicable to hybrid BESSs, where the SMs are integrated with heterogeneous energy storage. Experimental results are obtained to verify the effectiveness of the proposed algorithm and to compare its performance with respect to existing methods.**

***Index Terms*—Battery energy storage systems, cascaded H-bridge (CHB), state of charge.**

I. Introduction

THE share of renewable energy sources in global electricity generation has increased to 29% by 2020, where the solar photovoltaic (PV) and wind contribute two-thirds of the growth [1]. Consequently, battery energy storage systems (BESSs) are required in the power system to compensate for the intermittency and fluctuations in the generated renewable power [2]. The cascaded H-bridge (CHB) converter is a suitable candidate to integrate the BESS into the power system, especially in medium-/high-voltage applications [3]–[6]. Compared to the conventional two-level converters, advantages of the CHB converter include modularity, better harmonic performance, lower switching frequency, ability to accommodate heterogeneous energy storage, etc. [7]–[9].

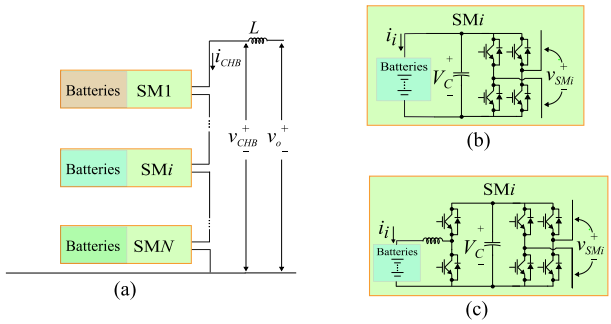

Fig. 1. Circuit diagram. (a) CHB converter-based BESS. (b) Battery modules directly connected to the SM. (c) Battery modules connected to the SM via a boost converter.

Fig. 1(a) depicts the circuit diagram of a single-phase CHB converter-based BESS, which consists of N submodules (SMs). Battery modules are integrated into the SMs directly or via a dc–dc converter, as depicted in Fig. 1(b) and (c) [10], respectively. Ideally, the battery modules of all the SMs are identical and operate symmetrically in a BESS, which is referred to as symmetric BESS in this article. There is also nowadays interest in hybrid BESSs, which consists of different battery modules and operates asymmetrically [11]. As an example, it is economic to use second-life batteries of electric vehicles, with different state of health (SoH), power rating, and capacity, etc. [12]. Another example is employing a proper combination of high-energy batteries and high-power batteries to effectively reduce the required number of batteries and cost of a BESS [13].

Despite the aforementioned benefits, hybrid BESSs present challenges, while balancing the state of charge (SoC) among the SMs within the phase arm. SoC balance is important as it enables a BESS to fully utilize its power and energy capacities [14]. For instance, without proper SoC balancing, the batteries in some SMs may be fully discharged much faster than the batteries in other SMs, leading to a reduced active power capacity.

Manuscript received January 16, 2022; revised March 22, 2022; accepted April 19, 2022. Date of publication April 26, 2022; date of current version June 24, 2022. This work was supported in part by the Office of Naval Research U.S. under DUNS Code: 595886219 and in part by the Spanish Centre for the Development of Industrial Technology through the "Cervera" Program under Grant CER-20191002 ENERISLA. Recommended for publication by Associate Editor G. Oriti. *(Corresponding author: Gaowen Liang.)*

Gaowen Liang and Josep Pou are with the School of Electrical and Electronic Engineering, Nanyang Technological University, Singapore 639798 (e-mail: gaowen001@e.ntu.edu.sg; josep.pou@ieee.org).

Ezequiel Rodriguez, Glen G. Farivar, and Naga Brahmendra Yadav Gorla are with the Energy Research Institute, Nanyang Technological University, Singapore 639798 (e-mail: ezequiel001@e.ntu.edu.sg; gfarivar@ntu.edu.sg; a0135566@u.nus.edu).

Salvador Ceballos is with Tecnalia, Basque Research and Technology Alliance, 48160 Derio, Spain (e-mail: salvador.ceballos@tecnalia.com).

Christopher D. Townsend is with the Department of Electrical, Electronic and Computer Engineering, University of Western Australia, Crawley, WA 6009, Australia (e-mail: townsend@ieee.org).

Color versions of one or more figures in this article are available at https://doi.org/10.1109/TPEL.2022.3170062.

Digital Object Identifier 10.1109/TPEL.2022.3170062

The conventional inter-SM SoC balancing methods for the CHB-based BESS can be classified into two main categories, viz., those based on proportional and integral (PI) controllers [15]–[17], and those using a sorting stage [18]–[20].

The PI-based methods [15]–[17] modify the output voltage references of the SMs by adding a fundamental-frequency voltage component, which is in phase with the arm current and whose amplitude is calculated with a PI controller according to the SoC unbalance among the SMs. The modification of SM output voltage references leads to different SM active powers, which balance the inter-SM SoCs. However, as the SM active power is implicitly modified by the PI controller, this category of methods lacks an explicit mechanism to constrain the active powers within safe operating ranges. Moreover, the design of the control gains in the PI controller is affected by the battery capacities of each SM [16], which makes it challenging to design the PI parameters when applied to hybrid BESSs as the battery capacities can vary among the SMs.

The sorting-based methods [18]–[20] first decide the number of SMs to insert and their polarity (either positive or negative) at each sampling period. Then, based on the SoC values of the SMs and the arm current direction, a sorting stage is used to choose which SMs to insert, which affects the SM active powers and hence balances the SoC. Similar to the PI-based methods, sorting-based methods also lack an explicit mechanism to constrain the SM active powers within safe operating ranges as the powers are implicitly modified by the sorting stage. Moreover, even with a mild SoC unbalance among the SMs, the sorting stage can significantly modify the SM active powers, hence some SMs will be charged/discharged with relatively large powers that can shorten the lifespan of batteries.

From the above discussion, there is a dearth of the inter-SM SoC balancing methods that can effectively balance the SoC, while constraining the active powers of the SMs within a safe range. To address this gap, this article first investigates the performance of the existing SoC balancing methods and reveals their drawbacks. Afterward, the article proposes a rule-based SoC balancing algorithm that overcomes the drawbacks of the existing methods without compromising the SoC balancing capability. The proposed algorithm is applicable to symmetric and hybrid BESSs, which makes it general.

The rest of this article is organized as follows. Section II examines the existing SoC balancing methods and reveals their drawbacks. Section III introduces the proposed rule-based method. Experimental results are provided in Section IV. Finally, Section V concludes the article.

II. Conventional SoC Balancing Methods

This section first introduces the principle of the SoC balancing. Afterward, the existing SoC balancing methods are reviewed.

A. SoC Balance

In a CHB converter-based BESS with N SMs per phase, which is depicted in Fig. 1(a), the SoC of the battery module in the ith ($i \in [1, N]$) SM is calculated using the Coulomb method [21]

$$\mathrm{SoC}_i(t) = \mathrm{SoC}_i(0) + \frac{\int_0^t i_i dt}{Q_i} \tag{1}$$

where $\mathrm{SoC}_i(t)$ and $\mathrm{SoC}_i(0)$ correspond to the instantaneous SoC and the initial SoC, respectively, i_i refers to the battery current, and Q_i denotes the capacity of the battery module. Note that SoC_i is within the range [0%, 100%]. Although i_i may contain considerable low- and high-frequency ripple, SoC_i can be considered free of the ripple as Q_i is usually large for batteries. The capacity Q_i corresponds to [22]

$$Q_i = Q_{\mathrm{nom}-i} \times \mathrm{SoH}_i \tag{2}$$

where $Q_{\mathrm{nom}-i}$ and SoH_i refer to the nominal capacity and SoH of the battery module in the ith SM, respectively.

The average value of i_i in a fundamental period corresponds to

$$\bar{i_i} = \frac{\bar{P}_{bi}}{V_{bi}} \tag{3}$$

where $\bar{P}_{bi}$ and V_{bi} are the average active power and voltage of the battery module in the ith SM, respectively. The value of $\bar{P}_{bi}$ depends on the average active power of the corresponding SM

$$\bar{P}_{bi} = \eta_i \bar{P}_i \tag{4}$$

where $\bar{P}_i$ refers to the average active power of the SM and η_i denotes the ratio of $\bar{P}_{bi}$ to $\bar{P}_i$. When $\bar{P}_i > 0$, which means the SM is charging, η_i is below one due to the power converter loss in the SM. When $\bar{P}_i < 0$, which means the SM is discharging, η_i may be one or higher than one [14]. The value of $\bar{P}_i$ corresponds to

$$\bar{P}_i = \frac{1}{T} \int_{t_0}^{t_0+T} v_{SMi} i_{\mathrm{CHB}} dt \tag{5}$$

where T refers to the fundamental voltage period, v_{SMi} refers to the output voltage of the ith SM, and i_{CHB} refers to the arm current of the CHB converter. Note that v_{SMi} is within $[-V_C, V_C]$, where V_C refers to the capacitor voltage. Moreover, v_{SMi} can differ among the SMs, thus providing a degree of freedom to modify the active power of each SM. In fact, the existing SoC balancing methods [15]–[19] modify the output voltage of the SMs based on their SoC values, leading to different battery currents, and hence different active powers, that aim at balancing the SoC values.

B. PI-Based Methods

PI-based methods [15]–[17] modify the output voltage references of the SMs by adding a fundamental-frequency voltage component, denoted as Δv_{SMi}, which is in phase with the arm current i_{CHB}. The amplitude of Δv_{SMi} is calculated by a PI controller according to the SM SoC unbalance.

As an example, Fig. 2(a) depicts the SoC balancing method in [16]. Denoting the mean SoC as $\overline{\mathrm{SoC}}$ ($\overline{\mathrm{SoC}} = \frac{1}{N}\sum_{i=1}^{N} \mathrm{SoC}_i$), the SoC unbalance of the ith SM corresponds to

$$\Delta\mathrm{SoC}_i = \overline{\mathrm{SoC}} - \mathrm{SoC}_i. \tag{6}$$

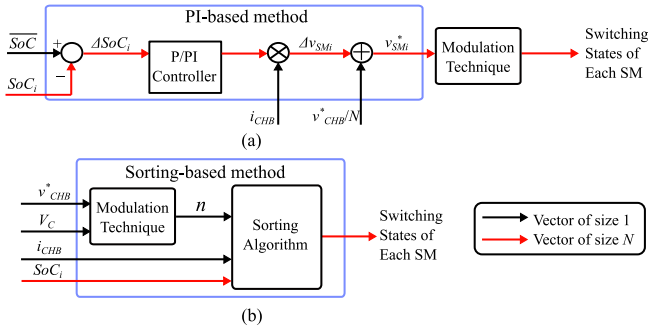

Fig. 2. Conventional SoC balancing methods. (a) PI-based method. (b) Sorting-based method.

The voltage component Δv_{SMi} is then calculated as

$$\Delta v_{SMi} = K_p \Delta \text{SoC}_i i_{\text{CHB}} \tag{7}$$

where K_p is the control gain. Thus, the product of Δv_{SMi} and i_{CHB} generates an active power proportional to ΔSoC_i that balances the SoC. Note that $\sum_{i=1}^{N} \Delta v_{SMi} = 0$ and hence, the total active power of the BESS is unaffected.

Although the results in [15]–[17] show that PI-based methods can balance the inter-SM SoC when applied to symmetric BESSs, they have some drawbacks as follows.

1) The output voltage of each SM is limited to a fundamental-frequency component only, which weakens the SoC balancing capability. According to [23], by adding components of other frequencies to the fundamental-frequency voltage, the SMs can process more active power. Accordingly, this article uses this ability to enhance SoC balancing capability.
2) It is difficult to limit the active power of each SM within a prescribed safe range since the active powers are indirectly affected by the output of the PI controller. The calculation of Δv_{SMi} does not consider its effect on the SM active power. Moreover, if a saturation stage is added to the output of the PI controller, the sum of SM output voltages can be different from the reference voltage of the converter, which affects the total active power of the BESS.
3) It is not trivial to design the PI parameters when applied to hybrid BESSs because the SoC balancing time constant is related to the battery capacities [16].

C. Sorting-Based Methods

Sorting-based methods [18], [19] use a sorting stage to decide the operation mode of each SM at each sampling step, according to their corresponding SoC and the arm current direction.

As an example, Fig. 2(b) depicts the SoC balancing method in [18]. According to the converter voltage reference v^*_{CHB} and the SM capacitor voltages V_C, the required number of SMs to insert is derived, and denoted as n ($n \in [1, N]$). Based on i_{CHB}, n, and the SoC of each SM, a sorting method is used to select the SMs to insert with a similar polarity to v^*_{CHB}. When v^*_{CHB} and i_{CHB} have similar polarities, which means the inserted SMs will be charged, the n SMs with the lowest SoC will be inserted, while the others will be bypassed. Otherwise, the n SMs with the highest SoC will be inserted, while the others will be bypassed.

Similar to the PI-based methods, the sorting-based methods cannot constrain the active power of each SM since the SM active power is not considered in the sorting stage. Moreover, with sorting-based methods, the SM output voltages normally have the same polarity as the converter voltage, which can weaken the active power capability of the SMs [23].

To conclude, the existing methods have important drawbacks that limit their application. To overcome the aforementioned drawbacks, a novel rule-based SoC balancing method is developed in the next section.

III. Proposed Rule-Based Method

The conventional inter-SM SoC balancing methods directly modify the SM output voltages v_{SMi} according to the SoC unbalances, which indirectly decide the active power distribution among the SMs. Consequently, the SM active powers can become unsafe. For example, charging an SM with a higher power than its rated value will damage the integrated batteries and switches. To overcome this challenge, the proposed method explicitly calculates the active power reference of each SM that balances their SoC values, with consideration of constraints in SM active powers. Moreover, the differences in the integrated battery modules (SoH, power rating, etc.) are considered in the calculation of the power references, which makes the proposed method general and suitable for hybrid BESSs.

A. SM Active Power Constraints

In the operation of a BESS based on the CHB converter, the constraints in the SM active powers can be classified into three different categories, which are referred in this article as hardware constraints, summation constraints, and disparity constraints.

1) Hardware Constraints: In practice, the maximum power that an SM can process is limited by its components, such as the integrated battery modules, the power switches, etc. The hardware constraints can be formulated as inequalities

$$\bar{P}_{li} \le \bar{P}^*_i \le \bar{P}_{ui} \forall i \in [1, N] \tag{8}$$

where $\bar{P}_{li}$ and $\bar{P}_{ui}$ refer to the lower and upper active power limits of the ith SM, respectively, while $\bar{P}^*_i$ denotes the power reference of the ith SM. Note that $\bar{P}_{li}$ and $\bar{P}_{ui}$ can differ among the SMs in a hybrid BESS. Violating the hardware constraints compromises the converter safety and operation.

2) Summation Constraint: The sum of the SM active power references must be equal to the total active power reference of the BESS, denoted as $\bar{P}^*_{\text{BESS}}$. Thus, the summation constraint corresponds to the following equality:

$$\sum_{i=1}^{N} \bar{P}^*_i = \bar{P}^*_{\text{BESS}}. \tag{9}$$

3) Disparity Constraints: According to the analysis in [23] and [24], there are constraints on the disparity among the SM active power references, i.e., there is an upper limit in the active power that can be processed by a certain number of SMs. The

disparity constraints can be formulated as [23]

$$\sum_{j=1}^{n} \bar{P}_j^* \leq \bar{P}_{\max}^n \forall n \in [1, N-1] \tag{10}$$

where $\bar{P}_j^*$ refers to the jth ($j \in [1, N]$) maximum active power reference, $\sum_{j=1}^{n} \bar{P}_j^*$ refers to the sum of the n largest power references, and $\bar{P}_{\max}^n$ denotes the maximum active power that can be processed by the n SMs. Note that $\bar{P}_j^*$ is different from $\bar{P}_i^*$, as $\bar{P}_i^*$ refers to the power reference of the ith SM. The derivation of $\bar{P}_{\max}^n$ is explained in [23] and [24] and hence not repeated in this article for the sake of simplicity. The value of $\bar{P}_{\max}^n$ is determined by the SM capacitor voltage, the converter output voltage and arm current. Unlike the hardware constraints, violating the disparity constraints involves unfeasible power references, i.e., the SMs will fail to track their corresponding power references, thus limiting the converter operation.

B. Unconstrained SoC Balancing Solution

This subsection explains how to calculate the active power reference for each SM that can balance their SoC values with consideration of the summation constraint (9). The hardware and disparity constraints will be incorporated in the subsequent stages.

From (3) and (4), the average battery current of a SM depends on the SM active power as

$$\bar{i}_i = \frac{\eta_i \bar{P}_i}{V_{bi}}. \tag{11}$$

Combining (1) and (11), the SoC dynamics correspond to

$$\mathrm{SoC}_i(t) = \frac{\eta_i \bar{P}_i}{Q_i V_{bi}} \tag{12}$$

Hence, the SoC values can be balanced via a proper allocation of the SM active power references.

To balance the SoC, the proposed method aims at steering the SoC of all the SMs to a prescribed reference value, SoC^*, simultaneously. From (12), when the ith SM is charged with a certain active power $\bar{P}_i$, the time for its SoC value to reach SoC^* will be

$$t_i = \frac{\mathrm{SoC}^* - \mathrm{SoC}_i}{\mathrm{SoC}_i}. \tag{13}$$

Substituting (12) into (13), it is derived that

$$t_i = \frac{E_i}{\bar{P}_i} \tag{14}$$

where

$$E_i = \frac{(\mathrm{SoC}^* - \mathrm{SoC}_i) Q_i V_{bi}}{\eta_i}. \tag{15}$$

Note that E_i corresponds to the energy required to steer SoC_i to SoC^*.

As the battery modules of all the SMs are expected to reach their corresponding SoC^* simultaneously, t_i should be similar for all the SMs

$$\frac{E_i}{\bar{P}_i} = T_C \forall i \in [1, N] \tag{16}$$

where $T_C > 0$ refers to the time to steer SoC_i to SoC^* for all the SMs. Combining (16) and the summation constraint in (9), the active power reference of each SM corresponds to

$$\bar{P}_i^* = \frac{E_i}{\sum_{i=1}^{N} E_i} \bar{P}_{\mathrm{BESS}}^*. \tag{17}$$

Note that in the proposed method, the SoC balancing speed is affected by the value of SoC^*. According to (15) and (17), (16) is rewritten as

$$T_C = \frac{1}{\bar{P}_{\mathrm{BESS}}^*} \sum_{i=1}^{N} \frac{(\mathrm{SoC}^* - \mathrm{SoC}_i(0)) Q_i V_{bi}}{\eta_i} \tag{18}$$

where $\mathrm{SoC}_i(0)$ refers to the initial SoC value. Hence, if there is a desired T_C, the value of SoC^* can be calculated by solving (18). When there is no specific requirement of T_C, SoC^* can be simply chosen as the allowed maximum SoC value (SoC_U) when $\bar{P}_{\mathrm{BESS}}^* > 0$ and simply chosen as the allowed minimum SoC value (SoC_L) when $\bar{P}_{\mathrm{BESS}}^* < 0$, which guarantees that the batteries in all the SMs can be fully charged/discharged simultaneously.

C. Hardware Constraints Incorporation

If the unconstrained SM active power references calculated according to (17) are outside the range $[\bar{P}_{li}, \bar{P}_{ui}]$ defined by (8), the hardware constraints are violated. In this condition, the SM active power references should be modified for a safe operation.

Assume that there are some power references higher than their corresponding upper bounds, whose indices i are grouped in the set X, and some power references lower than their corresponding lower bounds, whose indices i are grouped in the set Y, i.e.,

$$\begin{aligned} &\bar{P}_i^* > \bar{P}_{ui} \forall i \in X \\ &\bar{P}_i^* < \bar{P}_{li} \forall i \in Y \\ &\bar{P}_{li} \leq \bar{P}_i^* \leq \bar{P}_{ui} \forall i \notin X \cup Y. \end{aligned} \tag{19}$$

To satisfy the hardware constraints, the power references that are outside the range will be saturated to their corresponding bounds, i.e., $\bar{P}_{li}$ or $\bar{P}_{ui}$. This changes the sum of the power references. Hence, to compensate for this change and thus keep the sum of power references equal to $\bar{P}_{\mathrm{BESS}}^*$ in (9), an opposite change, denoted as $\Delta \bar{P}_h^*$, must be shared by the power references

$$\Delta \bar{P}_h^* = \sum_{i \in X} (\bar{P}_{ui} - \bar{P}_i^*) + \sum_{i \in Y} (\bar{P}_{li} - \bar{P}_i^*). \tag{20}$$

If $\Delta \bar{P}_h^* > 0$, which means that the power references need to be increased, $\Delta \bar{P}_h^*$ will be shared by those references that are below their upper bounds. Similarly, if $\Delta \bar{P}_h^* < 0$, $\Delta \bar{P}_h^*$ will be shared by those references that are above their lower bounds. A straightforward method would be to distribute $\Delta \bar{P}_h^*$ evenly among the power references. However, this even distribution cannot guarantee that the updated power references are within the safe range $[\bar{P}_{li}, \bar{P}_{ui}]$. For this reason, a method is proposed to distribute $\Delta \bar{P}_h^*$ according to the increase and decrease margins of the power references. The method aims at penalizing more the power references that are far from their corresponding bounds,

while penalizing less the references that are close to their bounds. The increase and decrease margins of the ith SM correspond to

$$IM_i = \bar{P}_{ui} - \bar{P}_i^* \tag{21}$$

$$DM_i = \bar{P}_i^* - \bar{P}_{li} \tag{22}$$

respectively.

If $\Delta\bar{P}_h^* > 0$, $\Delta\bar{P}_h^*$ will be distributed among the references according to their increase margins. Hence, each SM power reference will be increased by

$$\Delta\bar{P}_{hi}^* = \frac{IM_i}{\sum_{i=1}^{N} IM_i}\Delta\bar{P}_h^*. \tag{23}$$

Note that $\Delta\bar{P}_{hi}^*$ will be zero for those SMs whose active power references have reached their upper bounds since they cannot be further increased ($IM_i = 0$). Similarly, if $\Delta\bar{P}_h^* < 0$, each power reference will be decreased by

$$\Delta\bar{P}_{hi}^* = \frac{DM_i}{\sum_{i=1}^{N} DM_i}\Delta\bar{P}_h^*, i \in [1, N]. \tag{24}$$

Note that $\Delta\bar{P}_{hi}^*$ will be zero for those SMs whose active power references have reached their lower bounds since they cannot be further decreased ($DM_i = 0$).

D. Disparity Constraints Incorporation

Once the hardware constraints have been incorporated, then the SM power references need to be assessed in terms of the disparity constraints in (10). The updated SM power references according to (23) or (24) are first sorted in descending order, and then evaluated in (10) from $n = 1$ to $n = N - 1$. If the power references satisfy the $N - 1$ inequalities in (10), they can be allocated to the corresponding SMs. Otherwise, they need to be modified as follows.

As a general case, let us assume that the disparity constraints in (10) are satisfied for the $m - 1$ largest power references but violated for the m largest power references, which means

$$\sum_{j=1}^{n} \bar{P}_j^* \le \bar{P}_{\max}^n \forall n \in [1, m-1]$$

$$\sum_{j=1}^{m} \bar{P}_j^* > \bar{P}_{\max}^m. \tag{25}$$

Hence, to satisfy the disparity constraint when $n = m$, the m largest power references need to be reduced by at least

$$\Delta\bar{P}_d = \sum_{j=1}^{m} \bar{P}_j^* - \bar{P}_{\max}^m \tag{26}$$

where $\Delta\bar{P}_d > 0$. Accordingly, the remaining $N - m$ lowest power references need to be increased by $\Delta\bar{P}_d$ to guarantee that the sum of power references remains unchanged and equal to $\bar{P}_{\text{BESS}}^*$ in (9). For the sake of distinction, in this subsection the m largest power references are denoted as $\bar{P}_{j1}^*$, while the remaining $N - m$ lowest power references are denoted as $\bar{P}_{j2}^*$. Thus, $j1 \in [1, m]$ and $j2 \in [m + 1, N]$.

There are multiple methods to distribute the decrease of $\Delta\bar{P}_d$ among the m largest references $\bar{P}_{j1}^*$. However, to avoid violating the lower bounds of the hardware constraints, $\Delta\bar{P}_d$ will be distributed among the m references according to their corresponding decrease margins DM_{j1} in (22). Hence, $\bar{P}_{j1}^*$ will be updated as

$$\widehat{P}_{j1}^* = \bar{P}_{j1}^* - \Delta\bar{P}_d \frac{DM_{j1}}{\sum_{j1=1}^{m} DM_{j1}}, j1 \in [1, m] \tag{27}$$

where $\widehat{P}_{j1}^*$ represents the updated power reference of the $j1$th SM. Since $\Delta\bar{P}_d > 0$, the updated references $\widehat{P}_{j1}^*$ are below their corresponding original values $\bar{P}_{j1}^*$, i.e.,

$$\widehat{P}_{j1}^* \le \bar{P}_{j1}^* \forall j1 \in [1, m]. \tag{28}$$

Note that the values of $\bar{P}_{\max}^n$ are dependent on the operating condition of the converter and are not affected by the active power references of the SMs. Hence, as the original references $\bar{P}_{j1}^*$ satisfied the disparity constraints for $n \in [1, m-1]$, so will the updated references $\widehat{P}_{j1}^*$. Moreover, according to (26) and (27), the updated references $\widehat{P}_{j1}^*$ satisfy the disparity constraint in (10) for $n = m$, as their sum is saturated to $\bar{P}_{\max}^m$, i.e.,

$$\sum_{j1=1}^{m} \widehat{P}_{j1}^* = \bar{P}_{\max}^m. \tag{29}$$

After the m largest references ($\bar{P}_{j1}^*$) have been updated, the remaining references ($\bar{P}_{j2}^*$) should be updated to remain the total active power unaffected. The increase of $\Delta\bar{P}_d$ will be distributed among the remaining power references ($\bar{P}_{j2}^*$) according to their corresponding increase margins IM_{j2}. However, in this case, IM_{j2} of a SM is not only decided by the upper bound of its hardware constraint ($\bar{P}_{uj2}$) but also by the disparity constraints, as the disparity constraint can be violated when increasing a specific power reference. Note that this consideration is not needed when decreasing $\bar{P}_{j1}^*$ in (27) since decreasing power references does not compromise the disparity constraints.

For a general updated reference $\widehat{P}_{j2}^*$, the hardware constraint in (8) requires

$$\widehat{P}_{j2}^* \le \bar{P}_{uj2}. \tag{30}$$

Furthermore, the disparity constraint in (10) for $n = m + 1$ requires the sum of any $m + 1$ references to be below $\bar{P}_{\max}^{m+1}$. Hence, the sum of any updated power reference $\widehat{P}_{j2}^*$ and the m references $\widehat{P}_{j1}^*$ should be below $\bar{P}_{\max}^{m+1}$, i.e.,

$$\widehat{P}_{j2}^* + \sum_{j1=1}^{m} \widehat{P}_{j1}^* \le \bar{P}_{\max}^{m+1} \forall j2 \in [m+1, N]. \tag{31}$$

According to (29), (31) can be rewritten as

$$\widehat{P}_{j2}^* \le \bar{P}_{\max}^{m+1} - \bar{P}_{\max}^m. \tag{32}$$

Combining (32) and (30), the increase margins of references $\bar{P}_{j2}^*$ are derived as

$$IM_{j2} = \min(\bar{P}_{\max}^{m+1} - \bar{P}_{\max}^m, \bar{P}_{uj2}) - \bar{P}_{j2}^*. \tag{33}$$

Hence, $\bar{P}_{j2}^*$ will be updated as

$$\widehat{P}_{j2}^* = \bar{P}_{j2}^* + \Delta\bar{P}_d \frac{IM_{j2}}{\sum_{j2=m+1}^{N} IM_{j2}}, j2 \in [m+1, N]. \tag{34}$$

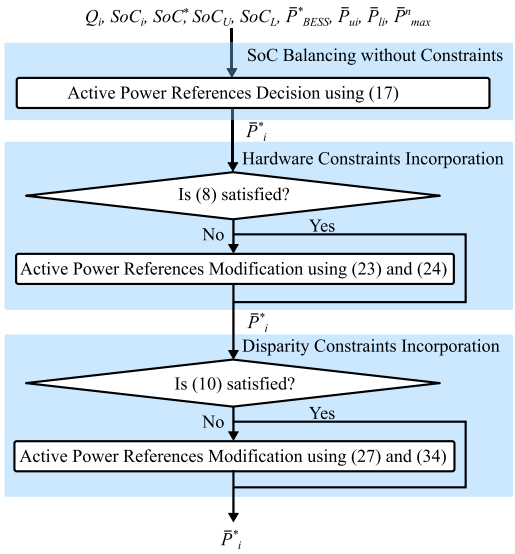

Fig. 3. Flowchart of the proposed rule-based SoC balancing method.

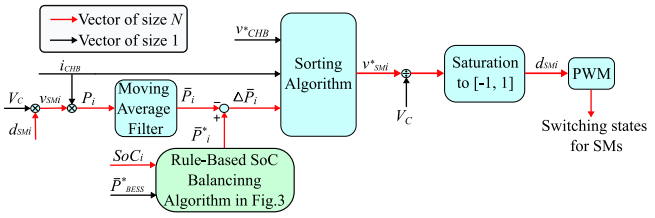

Fig. 4. SM power controller.

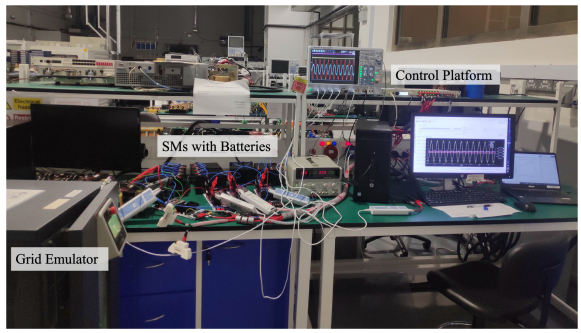

Fig. 5. Photo of the experimental prototype.

Note that since the increase/decrease to the SM power references in (27) and (34) may not be balanced, the descending order of the power references may change after an updating iteration, which could affect the satisfaction of the disparity constraints. If an updated reference $\widehat{P}^*_{j2}$ becomes larger than an updated reference $\widehat{P}^*_{j1}$, the disparity constraints for $n \in [1, m]$ in (10) can be violated as the m references $\widehat{P}^*_{j1}$ are not the largest power references. Therefore, to ensure the satisfaction of the disparity constraints after an iteration, $\widehat{P}^*_{j1}$ must remain the m largest power references, i.e.,

$$\widehat{P}^*_{j1} \geq \widehat{P}^*_{j2} \forall j1 \in [1, m] \wedge \forall j2 \in [m+1, N] \tag{35}$$

which in fact is fulfilled by the proposed method, and the proof is provided next.

As discussed, the updated references $\widehat{P}^*_{j1}$ satisfies the disparity constraints in (10) for $n = m - 1$, which means that the sum of any $m - 1$ references among them is below $\bar{P}^{m-1}_{\max}$

$$\left(\sum_{j1=1}^{m} \widehat{P}^*_{j1}\right) - \widehat{P}^*_{j1} \leq \bar{P}^{m-1}_{\max} \forall j1 \in [1, m]. \tag{36}$$

Combining (36) and (29) yields

$$\widehat{P}^*_{j1} \geq \bar{P}^{m}_{\max} - \bar{P}^{m-1}_{\max} \forall j1 \in [1, m]. \tag{37}$$

Besides, according to (32), each updated reference $\widehat{P}^*_{j2}$ is below $\bar{P}^{m+1}_{\max} - \bar{P}^{m}_{\max}$. According to the existing analysis in [25], it can be proved that

$$\bar{P}^{m}_{\max} - \bar{P}^{m-1}_{\max} \geq \bar{P}^{m+1}_{\max} - \bar{P}^{m}_{\max}. \tag{38}$$

Combining (32), (37), and (38), it can be proved that (35) is true.

To conclude, the overall flowchart of the proposed rule-based SoC balancing method, which calculates the SM active power references with consideration of the active power constraints, is depicted in Fig. 3. After the calculation of SMs active power references, a controller is required to regulate the SM active power.

In this article, the SM active power controller proposed in [23] is applied, which is depicted in Fig. 4. In this controller, a moving average filter is first used to calculate the average active power of each SM in a fundamental voltage period, denoted as $\bar{P}_i$. By comparing $\bar{P}_i$ with the corresponding references, the active power error is derived and denoted as $\Delta\bar{P}_i$. Based on $\Delta\bar{P}_i$, v^*_{CHB}, and i_{CHB}, a sorting stage is used to decide the output voltage reference of each SM (v^*_{SMi}). With the knowledge of v^*_{SMi}, a pulsewidth modulation (PWM) technique is applied to decide the switching state of each SM. Note that the major contribution of this article is the rule-based SoC balancing method, which provides the active power references of the SMs.

IV. Experimental Results

To verify the performance of the proposed SoC balancing method, experimental results are obtained on a hybrid BESS, where the capacity of battery modules are considerably different among the SMs. The CHB converter is built with Imperix PEH 2015 full-bridge power modules and connected to the Cinergia grid emulator through a filtering inductor. The Imperix B-Box RCP control platform is used to implement the control scheme. A picture of the setup is provided in Fig. 5. Parameters of the converter and battery modules are provided in Tables I and II, respectively.

A. Performance of the Proposed Method

To verify the performance of the proposed rule-based method, three different cases are tested in the experiments.

Case I : The first case investigates the ability of the proposed method to correct the power references when the hardware constraints are violated. In this specific case, the BESS is discharged with nominal power. The initial SoC values from SM1 to SM4 are 51.2%, 51.1%, 51.0%, and 50.9%, respectively. The power reference and measured active power of each SM are provided in

TABLE I
PARAMETERS OF THE EXPERIMENTAL BESS

Parameter	Value
Number of SMs per arm, N	4
SM capacitor voltage, V_C	50 V
SM capacitance, C	5 mF
Filter inductance, L	5 mH
Nominal output voltage (Peak), V_o	$110\sqrt{2}$ V
Nominal output current (Peak), I_{CHB}	$10\sqrt{2}$ A
Nominal output power, S_{nom}	1.1 kVA
Fundamental frequency, f	50 Hz

TABLE II
PARAMETERS OF BATTERY MODULES

Parameter	Allowed Power Range, $[\bar{P}_{li}, \bar{P}_{ui}]$	Allowed SoC Range	Capacity
Base value	1.1 kVA	1	7 Ah
SM1	$[-33\%, 15\%]$	$[20\%, 80\%]$	100%
SM2	$[-33\%, 15\%]$	$[20\%, 80\%]$	90%
SM3	$[-33\%, 15\%]$	$[20\%, 80\%]$	80%
SM4	$[-33\%, 15\%]$	$[20\%, 80\%]$	70%

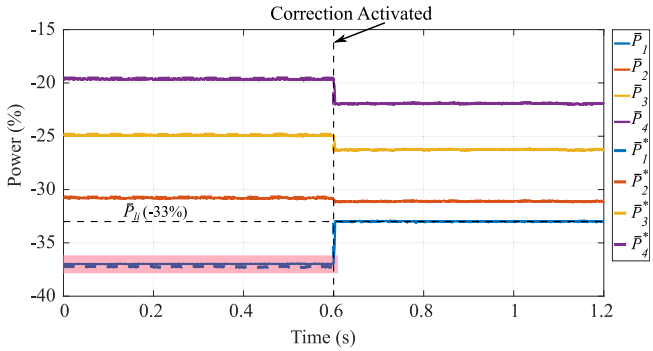

Fig. 6. *Case I* : Power references and measured powers of each SM when the hardware constraints are violated.

Fig. 6. Before the activation of the power references correction at t =0.6 s, as highlighted with red shading in the figure, the power reference and measured active power of SM1 are lower than its lower hardware limit ($\bar{P}_{l1} = -33\%$), which compromises the converter safe operation. After the activation, the active power reference of SM1 is increased and saturated at its lower limit, while the power references of the remaining SMs are decreased accordingly, which maintains the total active power of the BESS and avoids discharging the SM1 excessively. Furthermore, as observed, the decrease of active power references is distributed among the SMs according to their corresponding decrease margins (DM_i). For instance, the active power reference of SM4 decreases the most as its DM_i is the highest. This effectively guarantees that the updated power references do not violate the hardware constraints.

Case II : The second case investigates the ability of the proposed method to correct the power references when the disparity constraints are violated. The BESS is charged with 25% of the nominal power. The initial SoC values from SM1 to SM4

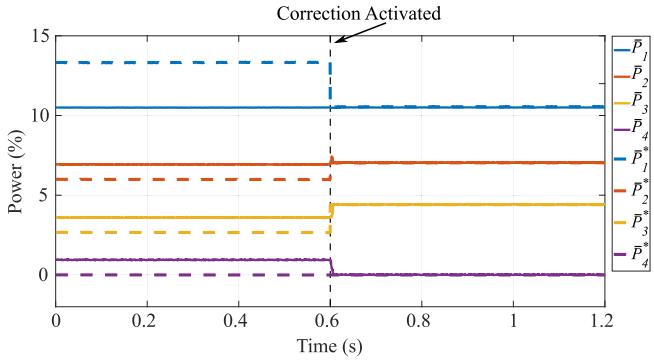

Fig. 7. *Case II* : Power references and measured powers of each SM when the disparity constraints are violated.

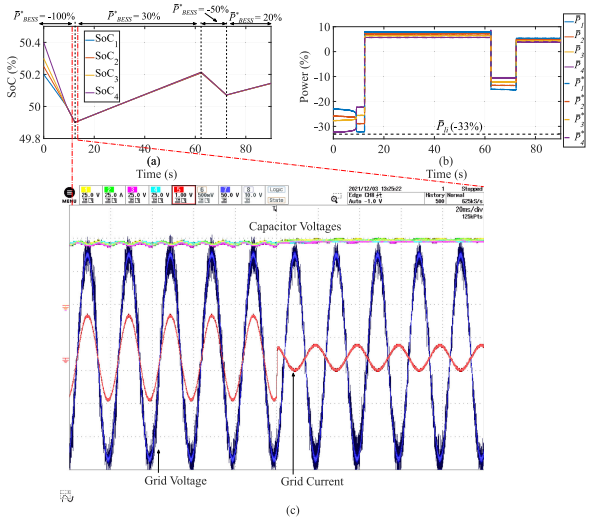

Fig. 8. *Case III* : Experimental results when the BESS is charged and discharged consecutively. (a) SoC of each SM. (b) Power references and measured powers of each SM. (c) Recorded capacitor voltages, grid voltage and current in the oscilloscope.

are 79.2%, 79.6%, 79.8%, and 80.0%, respectively. The power reference and measured active power of each SM are provided in Fig. 7. Before the activation of power reference correction at t =0.6 s, all the SMs fail to track their corresponding power references because they violate the disparity constraints. Moreover, although the SoC of SM4 has reached the allowed upper limit (80%), this SM is charging because it fails to track its power reference. After the activation, the SM power references are modified and the updated power references satisfy the disparity constraints. As observed, the measured power of each SM tracks its corresponding reference and SM4 is not charging.

Case III : The third case investigates the ability of the proposed method to balance the SoC values when the BESS is charged and discharged with different active power values consecutively. The results are provided in Fig. 8. According to Fig. 8(a), the SoC values of all the SMs reach balance at approximately t = 9 s, and then remain balanced despite the change of the BESS power. According to Fig. 8(b), each SM effectively tracks its corresponding active power reference and the SM active power is regulated within the safe range $[-33\%, 15\%]$. Fig. 8(c) depicts the recorded capacitor voltages, grid voltage, and arm current

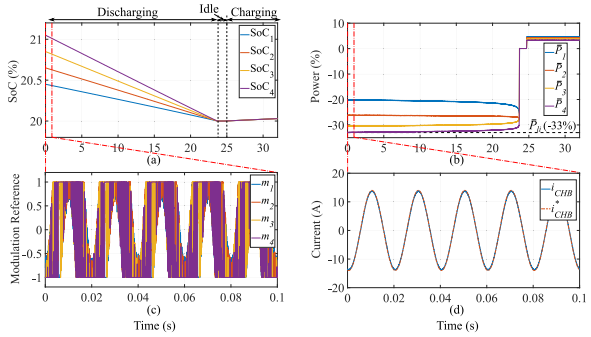

Fig. 9. Experimental results with the proposed rule-based method. (a) SoC of each SM. (b) Measured active powers of each SM. (c) Modulation reference. (d) Arm current.

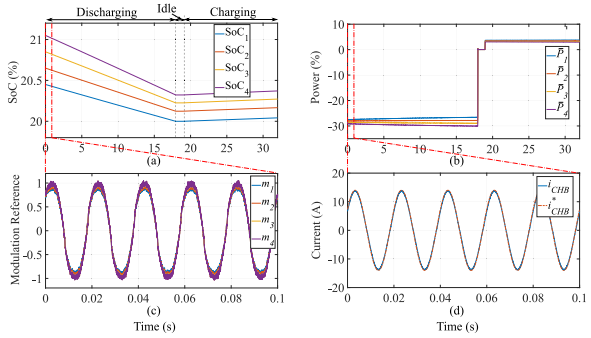

Fig. 10. Experimental results of the PI-based method without overmodulation. (a) SoC of each SM. (b) Measured active powers of each SM. (c) Modulation reference. (d) Arm current.

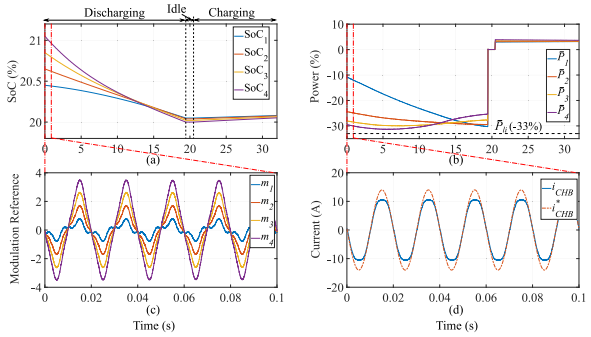

Fig. 11. Experimental results of the PI-based method with overmodulation. (a) SoC of each SM. (b) Measured active powers of each SM. (c) Modulation reference. (d) Arm current.

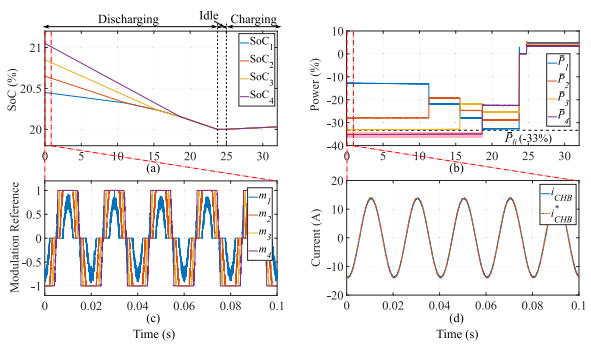

Fig. 12. Experimental results with the sorting-based method. (a) SoC of each SM. (b) Measured active powers of each SM. (c) Modulation reference. (d) Arm current.

in the oscilloscope when the BESS power changes from -100% (discharge) to 30% (charge).

To conclude, the proposed rule-based method can simultaneously balance the SoC values and regulate the SM active powers within a prescribed safe range.

B. Comparison With Different SoC Balancing Methods

This subsection compares the performances of the proposed method and the conventional methods. The BESS is first discharged with the nominal power and then charged with 20% of the nominal power. Results are provided in Figs. 9–12. The initial SoC values are unbalanced among the SMs.

Fig. 9 presents the results when the proposed rule-based method is implemented. Fig. 9(a) shows the SoC values of the SMs. As observed, the SoC values of all the SMs reach balance by the end of the discharging period. The active powers of the SMs are provided in Fig. 9(b), which are within their safe range. Fig. 9(c) provides the modulation references of each SM, which consist of some other harmonic components besides the fundamental one. Nevertheless, the harmonics cancel out, and hence the arm current of the CHB converter effectively tracks its reference, as Fig. 9(d) shows.

Fig. 10 presents the results when the PI-based method is implemented. The SM active powers are within the safe range and the arm current is well regulated, as observed from Fig. 10(b) and (d), respectively. However, according to Fig. 10(a), the SoC values do not reach balances. The SoC of the SM1 reached the allowed lower limit (20%) earlier than the remaining SMs and hence, the discharging process ends in advance without fully discharging the batteries. Note that in this case the PI controller is tuned to maximize the SoC balancing capability without causing overmodulation. As shown in Fig. 10(c), the modulation reference of SM1 has been maximized within $[-1, 1]$. These results show the reduced SoC balancing capability of the PI-based method.

The PI parameters can be further increased to pursue a better SoC balancing performance, and the results are provided in Fig. 11. According to Fig. 11(a) and (b), a better SoC balance is achieved and the SM active powers are still within the safe range. However, overmodulation occurs in SMs 2–4, as shown in Fig. 11(c). Consequently, the arm current cannot be regulated to its reference, as shown in Fig. 11(d).

Fig. 12 presents the results when the sorting-based method is implemented. As observed, the SoC balance is achieved, overmodulation is avoided, and the arm current is effectively regulated. However, the active power of SM1 is lower than its lower hardware limit during the discharging period, which is highlighted with red shading in Fig. 12(b).

A comparison of the computational burden among the methods is conducted on the control platform. The processor usage of the control platform is selected as the indicator of the computational burden and the results are provided in Fig. 13. Note that the worst scenario of the proposed method means that the originally preferred SM power references violate all the hardware and disparity constraints, while the best scenario means the original power references satisfy all the constraints.

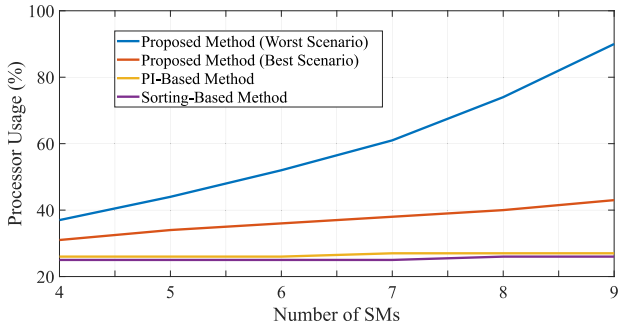

Fig. 13. Comparison of the computational burden between the existing and proposed methods.

TABLE III
COMPARISON OF THE SOC BALANCING METHODS

	Proposed	PI 1	PI 2	Sorting
SoC Balance Capability	High	Low	Low	High
Total Harmonic Distortion	Low	Low	High	Low
Computational Burden	High	Low	Low	Low
Power Constraints Satisfaction	Yes	No	No	No

From Fig. 13, the computational burden of the proposed method is heavier than the existing methods. This is because the proposed method needs to check the satisfaction of the different constraints, and modify the references when needed. If the proposed control method does not perform this correction duty, the system safety and operation are jeopardized, which is not desirable.

To conclude the experimental results, only the proposed rule-based method can balance the SoC without compromising the BESS operation, although it has a higher computational burden.

A brief comparison of all the SoC balancing methods studied in this article is shown in Table III, where the PI 1 and 2 correspond to the PI-based methods with and without overmodulation, respectively.

V. CONCLUSION

A rule-based method has been proposed to balance the SoC among the SMs within one arm of the CHB converter-based BESS. Compared to the conventional methods, the major advantage of the proposed algorithm is its ability to consider the SM active power constraints without compromising the SoC balancing performance. Moreover, the proposed method can consider the differences among battery modules, hence it is applicable to hybrid BESS applications. Experimental results have confirmed the effectiveness of the proposed algorithm and have shown its advantages compared to the conventional methods.

REFERENCES

[1] IEA, "Global energy review 2021: Renewables," 2021. [Online]. Available: https://www.iea.org/reports/global-energy-review-2021/renewables

[2] M. Sufyan, N. A. Rahim, M. M. Aman, C. K. Tan, and S. R. S. Raihan, "Sizing and applications of battery energy storage technologies in smart grid system: A review," *J. Renewable Sustain. Energy*, vol. 11, no. 1, Oct. 2019, Art. no. 014105.

[3] G. Wang *et al.*, "A review of power electronics for grid connection of utility-scale battery energy storage systems," *IEEE Trans. Sustain. Energy*, vol. 7, no. 4, pp. 1778–1790, Oct. 2016.

[4] Z. Li, R. Lizana, S. M. Lukic, A. V. Peterchev, and S. M. Goetz, "Current injection methods for ripple-current suppression in delta-configured split-battery energy storage," *IEEE Trans. Power Electron.*, vol. 34, no. 8, pp. 7411–7421, Aug. 2019.

[5] H. Mhiesan, Y. Wei, Y. P. Siwakoti, and H. A. Mantooth, "A fault-tolerant hybrid cascaded H-bridge multilevel inverter," *IEEE Trans. Power Electron.*, vol. 35, no. 12, pp. 12702–12715, Dec. 2020.

[6] Z. Li, R. Lizana, Z. Yu, S. Sha, A. V. Peterchev, and S. M. Goetz, "Modulation and control of series/parallel module for ripple-current reduction in star-configured split-battery applications," *IEEE Trans. Power Electron.*, vol. 35, no. 12, pp. 12977–12987, Dec. 2020.

[7] J. I. Leon, S. Vazquez, and L. G. Franquelo, "Multilevel converters: Control and modulation techniques for their operation and industrial applications," *Proc. IEEE*, vol. 105, no. 11, pp. 2066–2081, Nov. 2017.

[8] L. Zhang, Y. Tang, S. Yang, and F. Gao, "Decoupled power control for a modular-multilevel-converter-based hybrid AC-DC grid integrated with hybrid energy storage," *IEEE Trans. Ind. Electron.*, vol. 66, no. 4, pp. 2926–2934, Apr. 2019.

[9] J. Fang, Z. Li, and S. M. Goetz, "Multilevel converters with symmetrical half-bridge submodules and sensorless voltage balance," *IEEE Trans. Power Electron.*, vol. 36, no. 1, pp. 447–458, Jan. 2021.

[10] M. Vasiladiotis and A. Rufer, "Analysis and control of modular multilevel converters with integrated battery energy storage," *IEEE Trans. Power Electron.*, vol. 30, no. 1, pp. 163–175, Jan. 2015.

[11] S. Hajiaghasi, A. Salemnia, and M. Hamzeh, "Hybrid energy storage system for microgrids applications: A review," *J. Energy Storage*, vol. 21, pp. 543–570, Feb. 2019.

[12] I. Mathews, B. Xu, W. He, V. Barreto, T. Buonassisi, and I. M. Peters, "Technoeconomic model of second-life batteries for utility-scale solar considering calendar and cycle aging," *Appl. Energy*, vol. 269, pp. 115–127, Jul. 2020.

[13] T.-W. Noh, J.-H. Ahn, H. M. Ahn, and B. K. Lee, "Optimal design of hybrid battery energy storage system for minimizing the number of batteries with high efficiency control algorithm based on fuzzy logic," in *Proc. IEEE Appl. Power Electron. Conf. Expo.*, 2018, pp. 1630–1634.

[14] L. Xing *et al.*, "Distributed state-of-charge balance control with event-triggered signal transmissions for multiple energy storage systems in smart grid," *IEEE Trans. Syst., Man, Cybern.: Syst.*, vol. 49, no. 8, pp. 1601–1611, Aug. 2019.

[15] K. Kandasamy, D. Vilathgamuwa, and G. Foo, "Inter-module SoC balancing control for CHB based BESS using multi-dimensional modulation," in *Proc. Int. Conf. Ind. Technol.*, 2013, pp. 1630–1635.

[16] L. Maharjan, S. Inoue, H. Akagi, and J. Asakura, "State-of-charge (SoC)-balancing control of a battery energy storage system based on a cascade PWM converter," *IEEE Trans. Power Electron.*, vol. 24, no. 6, pp. 1628–1636, Jun. 2009.

[17] F. Gao, L. Zhang, Q. Zhou, M. Chen, T. Xu, and S. Hu, "State-of-charge balancing control strategy of battery energy storage system based on modular multilevel converter," in *Proc. IEEE Energy Convers. Congr. Expo.*, 2014, pp. 2567–2574.

[18] E. Chatzinikolaou and D. J. Rogers, "Cell SoC balancing using a cascaded full-bridge multilevel converter in battery energy storage systems," *IEEE Trans. Ind. Electron.*, vol. 63, no. 9, pp. 5394–5402, Sep. 2016.

[19] A. Moeini and S. Wang, "The state of charge balancing techniques for electrical vehicle charging stations with cascaded H-bridge multilevel converters," in *Proc. IEEE Appl. Power Electron. Conf. Expo*, 2018, pp. 637–644.

[20] C.-M. Young, N.-Y. Chu, L.-R. Chen, Y.-C. Hsiao, and C.-Z. Li, "A single-phase multilevel inverter with battery balancing," *IEEE Trans. Ind. Electron.*, vol. 60, no. 5, pp. 1972–1978, May 2013.

[21] M. A. Hannan, M. H. Lipu, A. Hussain, and A. Mohamed, "A review of lithium-ion battery state of charge estimation and management system in electric vehicle applications: Challenges and recommendations," *Renewable Sustain. Energy Rev.*, vol. 78, pp. 834–854, Oct. 2017.

[22] Z. Xia and J. A. A. Qahouq, "State-of-charge balancing of lithium-ion batteries with state-of-health awareness capability," *IEEE Trans. Ind. Appl.*, vol. 57, no. 1, pp. 673–684, Jan./Feb. 2021.

[23] G. Liang *et al.*, "Analytical derivation of inter-submodule active power disparity limits in modular multilevel converter-based battery energy storage systems," *IEEE Trans. Power Electron.*, vol. 36, no. 3, pp. 2864–2874, Mar. 2021.

[24] G. Liang *et al.*, "Effect of capacitor voltage ripples on submodule active power control limits of cascaded multilevel converters," *IEEE Trans. Ind. Electron.*, vol. 69, no. 6, pp. 5952–5961, Jun. 2021.
[25] G. Liang *et al.*, "Unbalanced active power distribution of cascaded multilevel converter-based battery energy storage systems," *IEEE Trans. Ind. Electron.*, to be published, doi: 10.1109/TIE.2021.3137442.

Gaowen Liang (Student Member, IEEE) received the B.Sc. degree in electrical engineering and automation from the South China University of Technology, Guangzhou, China, in 2018. He is currently working toward the Ph.D. degree in electrical engineering from Nanyang Technological University, Singapore.

His research interest includes multilevel power converters, energy storage systems, and electrical vehicles.

Ezequiel Rodriguez (Student Member, IEEE) was born in Tarragona, Spain, in 1994. He received the bachelor's degree in electrical engineering and the master's degree in engineering and technology of electronic systems (topping the 2012 and 2016 graduating cohorts as valedictorian) from Universitat Rovira i Virgili, Catalonia, Spain, in 2016 and 2017, respectively, and the Ph.D. degree in electrical engineering from Nanyang Technological University (NTU), Singapore, in 2022.

He is currently working as a Postdoctoral Research Fellow with the Energy Research Institute, NTU (ERI@N). His research interests include modelling and the control of power electronic converters, with an emphasis on modular multilevel cascade converters for energy storage and FACTS applications.

Glen G. Farivar (Senior Member, IEEE) received the B.Sc. degree in electrical engineering from the Nooshirvani Institute of Technology, Babol, Iran, in 2008, the M.Sc. degree in power electronics from the University of Tehran, Tehran, Iran in 2011, and the Ph.D. degree in electrical engineering from the University of NSW Australia, Syndey, NSW, Australia, in 2016.

He is currently working with Nanayang Technological University, Singapore, as a Senior Research Fellow with the Energy Research Institute (ERI@N) and a co-Director of Power Electronics and Applications Research Lab. He is a co-founder of SciLeap which aims to promote research integrity, accessibility, and openness. His research interests include renewable energy systems, high power convertors, energy storage, FACTS, and electric vehicles.

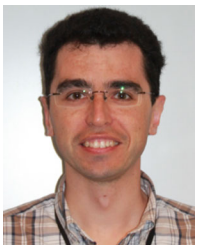

Salvador Ceballos received the M.S. degree in physics from the University of Cantabria, Santander, Spain, in 2001, and the M.S. and Ph.D. degrees in electronic engineering from the University of the Basque Country, Bilbao, Spain, in 2002 and 2008, respectively.

Since 2002, he has been with Tecnalia Research and Innovation, where he is currently a Principal Researcher with the Energy and Environment Division. His research interests include multilevel converters for high and medium voltage applications, fault-tolerant power electronic topologies, renewable energy systems and power systems with high penetration of power converters.

Christopher D. Townsend (Member, IEEE) received the B.E. and Ph.D. degrees in electrical engineering from the University of Newcastle, Callaghan, NSW, Australia, in 2009 and 2013, respectively.

He was with ABB Corporate Research, Väerås, Sweden, working on next-generation high-power converter technologies. Since then he has held various postdoctoral research positions with the University of New South Wales, Sydney, NSW, Australia, the University of Newcastle, Australia, and Nanyang Technological University, Singapore. In 2019, he joined the Department of Electrical, Electronic and Computer Engineering, University of Western Australia, Crawley, WA, Australia, as a Senior Lecturer. He has authored more than 60 published technical papers and has been involved in several industrial projects and educational programs in the field of power electronics. His research interests include topologies and modulation strategies for multilevel converters applied in power systems, renewable energy integration and electric vehicle applications.

Dr. Townsend is a Member of the IEEE Power Electronics and Industrial Electronics societies.

Naga Brahmendra Yadav Gorla (Member, IEEE) received the MS degree (by research) in electrical engineering from the Indian Institute of Technology Madras, Chennai, Tamil Nadu, India, in 2013, and Ph.D. degree in electrical engineering from the National University of Singapore, Singapore, in 2019.

He was with Electrical and Electronics Department, Singapore Polytechnic, Singapore, as Research Engineer, between October 2013 and December 2015. He was working as Research Fellow with Sembcorp-NUS Corporate laboratory, National University of Singapore, Singapore, between April 2019 and July 2020. He is currently working as a Research Fellow with Energy Research Institute, Nanyang Technological University (ERI@N), Singapore. His research interests include power quality improvement in grid connected inverters and rectifiers, common-mode and differential-mode noise, fault tolerance and resiliency in modular power electronic converters, solid-state-transformer architectures and their control strategies.

Josep Pou (Fellow, IEEE) received the B.S., M.S., and Ph.D. degrees in electrical engineering from the Technical University of Catalonia (UPC)-Barcelona Tech, Barcelona, Spain, in 1989, 1996, and 2002, respectively.

In 1990, he joined the faculty of UPC as an Assistant Professor, where he became an Associate Professor, in 1993. From February 2013 to August 2016, he was a Professor with the University of New South Wales (UNSW), Sydney, NSW, Australia. He is currently a Professor with the Nanyang Technological University (NTU), Singapore, where he is a Cluster Director of Power Electronics with the Energy Research Institute, NTU (ERI@N) and co-Director of the Rolls-Royce, NTU Corporate Lab. From February 2001 to January 2002, and February 2005 to January 2006, he was a Researcher at the Center for Power Electronics Systems, Virginia Tech, Blacksburg. From January 2012 to January 2013, he was a Visiting Professor with the Australian Energy Research Institute, UNSW, Sydney. He has authored more than 400 published technical papers and has been involved in several industrial projects and educational programs in the fields of power electronics and systems. His research interests include modulation and control of power converters, multilevel converters, renewable energy, energy storage, power quality, HVdc transmission systems, and more-electrical aircraft and vessels.

Dr. Pou is the recipient of the 2018 IEEE Bimal Bose Award for Industrial Electronics Applications in Energy Systems. He is currently an Associate Editor for the IEEE JOURNAL OF EMERGING AND SELECTED TOPICS IN POWER ELECTRONICS. He was co-Editor-in-Chief and Associate Editor for the IEEE TRANSACTIONS ON INDUSTRIAL ELECTRONICS.